CrystEngComm

Cite this: *CrystEngComm*, 2011, **13**, 2425

www.rsc.org/crystengcomm

**PAPER**

# Microwave-assisted synthesis of a biocompatible polyacid-conjugated $Fe_3O_4$ superparamagnetic hybrid

**Shanhu Liu,[ab] Feng Lu,[a] Xiangdong Jia,[a] Fangfang Cheng,[a] Li-Ping Jiang[a] and Jun-Jie Zhu*[a]**

***Received 4th August 2010, Accepted 23rd December 2010***
**DOI: 10.1039/c0ce00491j**



A rapid microwave-assisted method was developed for the facile synthesis of a polyacid-conjugated $Fe_3O_4$ superparamagnetic hybrid. Field-emission scanning electron microscopy, transmission electron microscopy, X-ray photoelectron spectroscopy, Fourier transform infrared spectroscopy, thermogravimetric and magnetic measurements, and a cytotoxicity assay were used to characterize the morphologies, structures, compositions and properties of the polyacid-conjugated $Fe_3O_4$ superparamagnetic hybrid. The hybrid is composed of superparamagnetic magnetite nanograins and presents a cluster-like structure; and its size range can be tuned from about 100 to 400 nm by varying the amount of $FeCl_3$ in the system. The hybrid not only exhibits excellent magnetic properties, good biocompatibility, and high water-dispersibility, but also facilitates further coupling interaction with some guest molecules because of the abundant existence of uncoordinated carboxylate groups on its surface.

## 1. Introduction

Superparamagnetism is of great significance as a small length-scale phenomenon of magnetic materials and has enabled tremendous advances in the development of powerful tools for separating, detecting and loading targets of interest in scientific research and technological applications.[1–5] For example, magnetic cell isolation with superparamagnetic nanoparticles is becoming increasingly important in a variety of biomedical fields such as drug screening, disease diagnosis and treatment. However, their practical applications are largely limited by the inadequate magnetization and complicated surface functionalization processes.[6–8]

To date, several strategies have been developed for the preparation of superparamagnetic nanoparticles, and examples include co-precipitation, thermal decomposition, microemulsion and hydrothermal reactions.[9–14] Among them, superparamagnetic nanoparticles prepared by co-precipitation often have polydisperse dimensions and result in agglomeration, which exhibit non-ideal magnetic behavior in applications.[8] Thermal decomposition of organometallic precursors affords monodisperse superparamagnetic nanoparticles but these particles are usually dispersible in organic solvent.[15] The transformation from hydrophobic particles to hydrophilic ones is indispensable by replacing the surface ligands with some hydrophilic bifunctional molecules for biomedical applications. However, ligand exchange not only makes the process complicated but also affects the quality of the nanoparticles.[16,17] On the other hand, due to their small size, most of the superparamagnetic nanocrystals possess too weak magnetic response to separate particles from solution or manipulate them in blood by using moderate magnetic fields.[8,18] Therefore, the fabrication of superparamagnetic magnetite nanoparticles with excellent magnetic responsiveness and abundant reactive groups on the surface is urgently needed for biomedical analyses and clinical applications.

Microwave heating has been accepted as a promising method for efficient and uniform heating of the solution, because it offers more homogeneous nucleation and shorter crystallization time as compared to conventional heating, which is greatly advantageous for the preparation of uniform and monodisperse nanoclusters. In the last few years, we have synthesized a series of nanomaterials through microwave procedures.[19–24] We report here the rapid synthesis of the polyacid-conjugated $Fe_3O_4$ superparamagnetic hybrid based on the microwave-assisted method. The hybrid exhibits significant magnetization, good biocompatibility and high water-dispersibility due to the involvement of the polyacid molecules of its surface. The involved-polyacid molecules further provide advantageous functionality for the linkage of some guest molecules such as antibodies, drugs and proteins, which could be promising in biomedical applications such as magnetic separation, targeted drug delivery, and microchip technology.[25]

## 2. Experimental section

### 2.1. Materials

Polyelectrolytes such as polyacrylic acid (PAA, 35%, w/w in water, MW = 100 000), poly(diallyldimethylammonium

[a]*Key Lab of Analytical Chemistry for Life Science (MOE), School of Chemistry and Chemical Engineering, Nanjing University, Nanjing, 210093, P.R.China. E-mail: jjzhu@nju.edu.cn; Fax: +86 25 83594976; Tel: +86 25 83594976*
[b]*Institute of Environmental and Analytical Sciences, College of Chemistry and Chemical Engineering, Henan University, Kaifeng 475004, P.R.China*

chloride) (PDDA, 20%, w/w in water, MW = 200 000–350 000), poly(allylamine hydrochloride) (PAH, MW = 15 000) and poly(sodium 4-styrenesulfonate) (PSS, MW = 70 000) were purchased from Sigma-Aldrich. Ferric chloride hexahydrate ($FeCl_3 \cdot 6H_2O$), anhydrous sodium acetate (NaAc), ethylene glycol (EG) and other chemical reagents were obtained from Nanjing Chemical Reagent Co., Ltd. All chemicals were directly used as received without further purification.

### 2.2. Fabrication of the polyacid-conjugated $Fe_3O_4$ superparamagnetic hybrid

The hybrid was synthesized in one pot *via* a microwave-assisted method in a microwave accelerated reaction system (CEM-Discover, USA). In a typical procedure, different amounts of $FeCl_3 \cdot 6H_2O$ (0.7, 1.5, 3.0, 5.0 mmol) were dissolved in 40 mL of EG to form a clear solution, followed by the addition of 1 ml of PAA and 20 mmol of anhydrous NaAc. The mixture was ultrasonicated vigorously to give a homogeneous solution. Then the solution was sealed in autoclaves (80 mL capacity) and irradiated to 200 °C for 50 min. The black solid products were collected by magnetic separation and washed at least three times with water and ethanol, then dried under vacuum at room temperature.

### 2.3. Cytotoxicity assay

The cytotoxicity study was carried out using the 3-(4,5-dimethylthiazol-2-yl)-2,5-diphenyltetrazolium bromide (MTT) assay on human cervical carcinoma HeLa cells. The MTT assay was carried out referencing to the literature method.[26] Briefly, HeLa cells were seeded in 96-well plates at $5 \times 10^3$ cells per well in DMEM medium and incubated at 37 °C in a humidified atmosphere with 5% $CO_2$ for 12 h. The cells were then treated in triplicate with fresh medium containing grade concentrations (0.05, 0.25, 1.00 mg $mL^{-1}$) of the hybrid with different sizes at 37 °C for 6 h, 12 h and 24 h, respectively. Aliquots of MTT (10 μL, 5 mg $mL^{-1}$) were added to each of the wells for 4 h of incubation. After the medium was removed, 150 μL of DMSO was added to each well. The absorbance of the purple formazan was recorded at 490 nm using an ELISA plate reader. The cytotoxicity results were calculated based on the data of three replicate tests.

### 2.4. Characterization

Field emission scanning electron microscopy (FE-SEM) images were obtained using a Hitachi S-4800 field emission electron microscope at an accelerating voltage of 5 kV. Transmission electron microscopy (TEM) images and selected area electron diffraction (SAED) patterns were taken using a JEOL JEM-2100 transmission electron microscope at an accelerating voltage of 200 kV. X-Ray powder diffraction (XRD) measurements were performed on a Japan Shimadzu XRD-6000 diffractometer with Cu-K$\alpha$ radiation ($\lambda = 0.15418$ nm); a scanning rate of 0.05 deg $s^{-1}$ was applied to record the patterns in the $2\theta$ range of 10–80°. X-Ray photoelectron spectra (XPS) were obtained using a Thermo ESCALAB 250 electron spectrometer with 150 W monochromatized Al K$\alpha$ radiation (1486.6 eV); the binding energy of the C1s level from contamination of saturated hydrocarbons at 284.8 eV was used as an internal reference to calibrate the spectra. FTIR spectra were recorded on a Nicolet 6700 Fourier transform infrared spectrograph in the wavenumber range of 4000–400 $cm^{-1}$. Zeta potentials ($\zeta$) were measured in pure water on a Malven Nano-Z instrument. Superconducting quantum interference device (SQUID, Quantum Design) magnetometer was used in the magnetic measurement at 300 K. Thermal gravimetric analysis (TGA) was carried out on a Pyris 1 TGA instrument with a heating rate of 20 °C $min^{-1}$ in a nitrogen flow (20 mL $min^{-1}$).

## 3. Results and discussion

As mentioned in the experimental section, the synthesis was performed in one pot with thorough dissolution of $FeCl_3$, NaAc and PAA in the EG. $FeCl_3 \cdot 6H_2O$ and anhydrous NaAc were used as the reactants; and EG served as polar solvent and reductant. PAA could not only coordinate with iron ions to regulate the grain size but also favorably endowed the dispersibility of the nanoclusters in water.[7]

The size and shape of the products were examined by SEM. As shown in Fig. 1(A–D), each of the samples is composed of spherical or quasi-spherical aggregates and exhibits a monodisperse population with narrow size distribution. The dimensions of the aggregates were statistically determined as 100, 180, 310 and 400 nm, corresponding to the initial iron amount of 0.7, 1.5, 3.0 and 5.0 mmol, respectively. Detailed structural information of the hybrid was obtained by TEM. Shown in Fig. 2A, the hybrid is structurally uniform and monodisperse. An enlarged TEM image in Fig. 2B shows that it is made up of primary nanograins (*ca.* 10 nm) and exhibits a cluster-like structure. The SAED patterns (inset of Fig. 2A) reveal that the hybrid is crystalline and is indexed to cubic phase magnetite. The high-resolution TEM image in Fig. 2C exhibits clear lattice fringes and these primary grains attached to each other with a common crystallographic orientation. The experimental lattice spacings of 0.256 nm are analogous to the (311) planes of cubic magnetite (0.253 nm).

The crystalline structures and phase composition of the hybrid with different sizes were characterized by XRD. As shown in

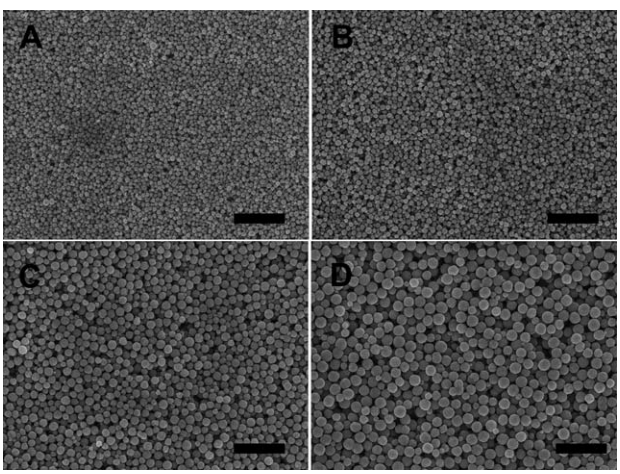


**Fig. 1** Typical SEM images of the PAA-$Fe_3O_4$ hybrid with different initial iron amounts of 0.7 mmol (A), 1.5 mmol (B), 3.0 mmol (C), and 5.0 mmol (D). All of the scale bars are 2 μm.

 

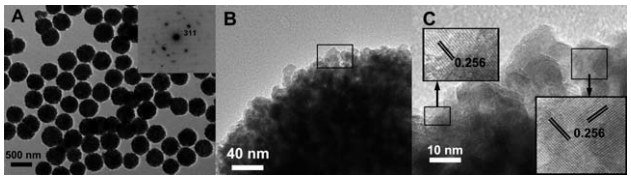


**Fig. 2** Representative TEM (A and B), SAED patterns (inset of A) and high-resolution TEM image (C, from the boxed region of B) of the hybrid with the diameter of about 400 nm.

Fig. 3A, all of the reflections are indexed to cubic structure of magnetite, in good agreement with the reported data (JCPDS No. 01-1111). Calculations with the Debye–Scherrer formula for the strongest reflections (311) give the crystal sizes of 10, 12, 13 and 14 nm for 100, 180, 310 and 400 nm, respectively. This evidence indicates that these primary particles did not grow significantly with the increase in the hybrid size. As magnetite ($Fe_3O_4$) and maghemite ($\gamma$-$Fe_2O_3$) have similar XRD patterns and both of them exhibit magnetic behavior, the composition of the products could be further identified by XPS spectroscopy. The Fe 2p high resolution XPS spectra reveal that Fe 2p has the binding energy values of 710.8 eV and 724.6 eV for 2p3/2 and 2p1/2, respectively, as shown in Fig. 3B. These values are close to that published in the literature for $Fe_3O_4$.[27,28] Furthermore, the absence of shake-up satellites between the two Fe 2p peaks excludes the possible presence of $\gamma$-$Fe_2O_3$.[6,27]

FTIR spectra were applied to detect the species on the surface of the hybrid. The FTIR spectra of pure PAA (curve A in Fig. 4) present a strong peak at 1716 $cm^{-1}$, which is assigned to the carbonyl stretching mode for protonated carboxylate groups (–COOH); but this peak is negligible in the spectra of the hybrid (curve B in Fig. 4). In addition, the IR peaks of the hybrid at 1411, 1453 and 1561 $cm^{-1}$ could be attributed to the vibration of symmetric C–O stretching, $CH_2$ bending, and asymmetric C–O stretching, respectively; all of which are characteristic bands of carboxylate groups ($–COO^-$). Furthermore, from the TGA data in Fig. 5, the weight loss of PAA at 150–200 °C is believed to be the decarboxylation process, accompanied with the release of $CO_2$ molecules (curve A).[29] For the hybrids, the larger the hybrid size, the less the weight loss of the hybrid, suggesting that there is a smaller weight fraction of PAA in the hybrid. This evidence based on the FTIR and TGA data indicates that the carboxylic acid groups (–COOH) of PAA have been decomposed or transformed into carboxylate groups ($–COO^-$) during the synthesis and the surface of the hybrid is mostly carboxylate groups.[7] This also explains why the FTIR spectrum of the hybrid only shows a weak carbonyl band at 1710 $cm^{-1}$. The results are

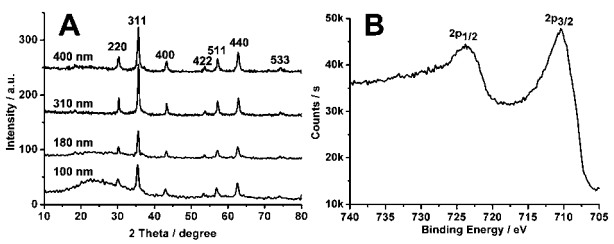


**Fig. 3** XRD patterns of the hybrid with different sizes (A) and Fe 2p high resolution XPS spectra of the hybrid with the diameter of 400 nm (B).

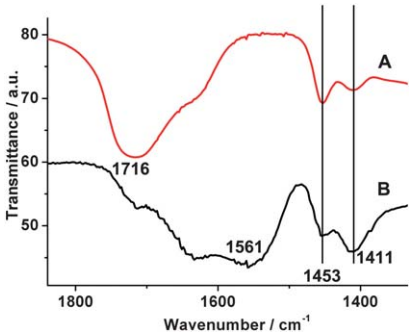


**Fig. 4** FTIR spectra of pure PAA (A) and the hybrid with the diameter of 400 nm (B).

further confirmed by the measurements of zeta potential (Table 1). All of the four sizes of the hybrid display abundant negative surface charges. However, their surface charge is negatively correlated with the hybrid size, due to the decrease in their corresponding specific surface area. In short, the hybrid was proven to be a complex of PAA and magnetite nanograins, and abundant carboxylate moieties on the hybrid surface ensure they possess surface reactive functionality, which would be available in biomedical applications.

The magnetic response properties of the hybrid were performed on SQUID. Fig. 6A and 6B show magnetization curves of the hybrids with different sizes at 300 and 1.8 K, respectively. At 300 K, the saturation values are 58.8, 65.3, 72.0 and 76.9 emu $g^{-1}$ for 100, 180, 310 and 400 nm, respectively, which are higher than those in the previous reports.[30–32] Furthermore, the zoomed area at low magnetic field (inset of Fig. 6A) demonstrates that all of the four sizes of the hybrid display superparamagnetic properties and no remanence or coercivity is observed. At 1.8 K, the thermal energy is insufficient to induce moment randomization so that the hybrids show typical ferromagnetic hysteresis loops with obvious remanence and coercivity (Fig. 6B and its inset).[7] The hybrid exhibits high dispersibility in water (Fig. 6C) and responds quickly even when a magnet is applied up to a distance of about 6 cm from the vial (Fig. 6D). The superparamagnetic properties might avoid magnetic agglomeration once the magnetic field is removed. Therefore, the excellent responsiveness and superparamagnetic properties would be beneficial to further applications in biotechnology *in vivo*.[33] In short, with superparamagnetic properties and excellent responsiveness, the hybrid could be a promising material for rapid separation and easy detection by virtue of magnetic force; this would facilitate

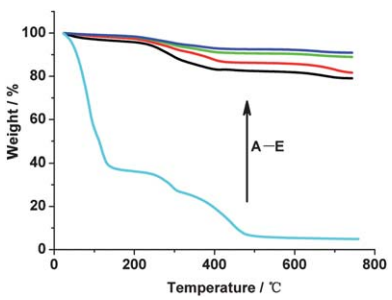


**Fig. 5** TGA curves of PAA (A) and the hybrid with diameters of 100 nm (B), 180 nm (C), 310 nm (D) and 400 nm (E).

**Table 1** Zeta potential data of the hybrids with different sizes

| Cluster size of the hybrids/nm | 100 | 180 | 310 | 400 |
|---|---|---|---|---|
| $\xi$ potential/mV | −41.8 | −39.6 | −37.8 | −32.9 |

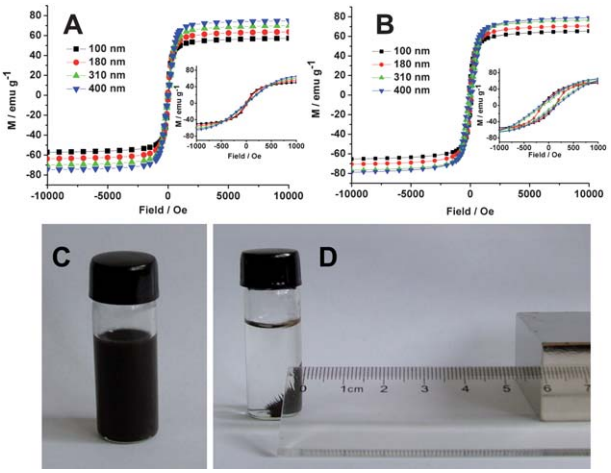


**Fig. 6** Magnetization curves of the hybrids with different sizes at a temperature of (A) 300 K and (B) 1.8 K. Insets show the data around zero field with an expanded scale ranging from −1000 to 1000 Oe. Photographs of a solution of the hybrid with the diameter of 400 nm in the absence (C) and presence (D) of a magnet.

their applications in catalysis, drug delivery, and protein and cell separation.[34,35]

To investigate the influence of PAA on the formation of the hybrids, two sets of control experiments were carried out as follows. Control A was to prepare magnetite in the presence of other polyelectrolytes instead of PAA, such as PDDA, PAH, PSS. Control B was to vary the amount of PAA. Each control experiment was performed in the same conditions and procedure as the typical experiments.

In the control A experiment, the products were composed of larger building blocks rather than nanograins, similar to the case without polyelectrolytes, indicating that the presence of abundant carboxylate groups is essential for the formation of the superparamagnetic hybrids (Fig. 7A–D). The influence of PAA on the morphology of the products was also investigated. When the PAA amount was 0.1 ml and 0.5 ml, the products had a good dispersion in water; but the crystal sizes of the building blocks were larger than those of the hybrid in the typical experiment, which might lead to ferromagnetic behavior (Fig. 8A–B). When the amount of PAA was up to 2 ml, the product was gelatiniform and its SEM image shows that the product displays vague cluster-like structures due to the poor conductivity of the excessive amount of organic matter attached on the product (Fig. 8C). Thus the PAA and its concentration are critical for the synthesis of the superparamagnetic hybrids.

The cytotoxicity of the hybrid was tested on the human cervical cancer cell line HeLa by MTT assay. Fig. 9 shows the cellular viability of HeLa cells with different concentrations of the four sizes of the hybrid for different incubation intervals. The viability of untreated cells was assumed to be 100%. When the hybrid size is less than 200 nm, the hybrid exhibits a negligible

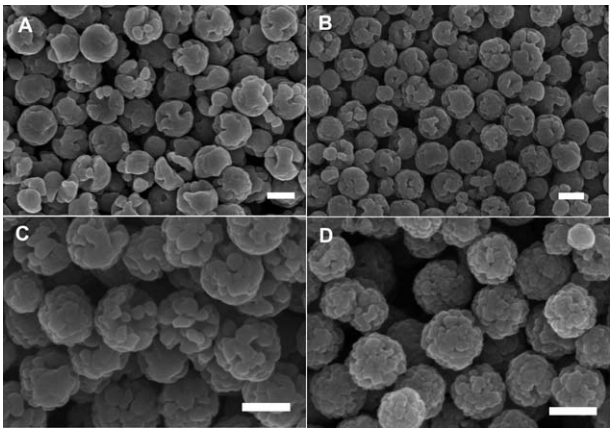


**Fig. 7** SEM images of the products obtained in the presence of other polyelectrolytes: 1 ml of PDDA (A), 0.1 g of PAH (B), 1 ml of PSS (C), and in the absence of any polyelectrolytes (D). All of the scale bars are 200 nm.

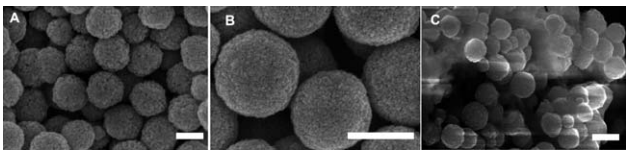


**Fig. 8** SEM images of the products prepared with varied initial amounts of PAA. 0.1 ml (A), 0.5 ml (B), and 2 ml (C). All of the scale bars are 200 nm.

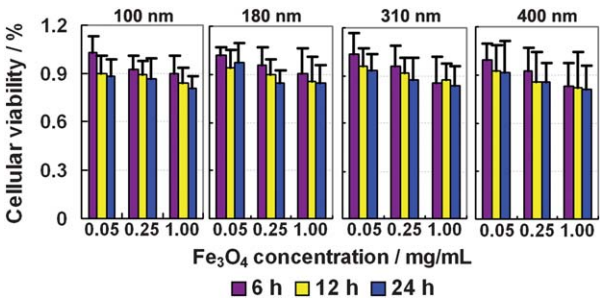


**Fig. 9** Cytotoxicity of the hybrids with different sizes against human cervical cancer cell line HeLa at concentrations of 0.05–1.00 mg $mL^{-1}$ after 6, 12, 24 h, with untreated cells as a negative reference: hybrid with the diameter of 100 nm (A), 180 nm (B), 310 nm (C) and 400 nm (D).

cytotoxic profile even after 24 h. Furthermore, over 80% cell viability was obtained when treated with 1.00 mg $mL^{-1}$ of the hybrid. This suggests that the hybrid exhibits good biocompatibility and would be practicable in applications in bio-related fields.

## 4. Conclusions

In summary, the polyacid-conjugated $Fe_3O_4$ superparamagnetic hybrid was conveniently fabricated by the introduction of a microwave-assisted method. The hybrid is composed of superparamagnetic magnetite nanograins and presents a cluster-like structure; and its size range can be tuned from about 100 to 400 nm by varying the amount of $FeCl_3$ in the system. The hybrid

 

exhibits excellent magnetic responsiveness and good biocompatibility, but offers advantageous functionality due to the preferential exposure of uncoordinated carboxylate groups on its surface. This avoids complicated functionalization processes and enhances the inefficiency of weak magnetization in manipulation in previous reports. This work provides a new insight into the preparation of superparamagnetic magnetite hybrids, which would have great potential for biomedical applications such as bio-separation, targeted drug delivery, cancer diagnosis and treatment, and microchip technology.

## Acknowledgements

We greatly appreciate the support of the National Natural Science Foundation of China for the Key Program (20635020), Creative Research Group (20821063). This work is also supported by National Basic Research Program of China (2011CB933502, 2007CB936404).

## Notes and references

1 S. H. Sun, C. B. Murray, D. Weller, L. Folks and A. Moser, *Science*, 2000, **287**, 1989.
2 C. J. Xu, K. M. Xu, H. W. Gu, R. K. Zheng, H. Liu, X. X. Zhang, Z. H. Guo and B. Xu, *J. Am. Chem. Soc.*, 2004, **126**, 9938.
3 M. J. Hu, Y. Lu, S. Zhang, S. R. Guo, B. Lin, M. Zhang and S. H. Yu, *J. Am. Chem. Soc.*, 2008, **130**, 11606.
4 C. H. Yang, K. S. Huang, Y. S. Lin, K. Lu, C. C. Tzeng, E. C. Wang, C. H. Lin, W. Y. Hsu and J. Y. Chang, *Lab Chip*, 2009, **9**, 961.
5 M. Arruebo, R. Fernandez-Pacheco, M. R. Ibarra and J. Santamaria, *Nano Today*, 2007, **2**, 22.
6 X. Jia, D. Chen, X. Jiao and S. Zhai, *Chem. Commun.*, 2009, 968.
7 J. P. Ge, Y. X. H. M. Biasini, C. L. Dong, J. H. Guo, W. P. Beyermann and Y. D. Yin, *Chem.–Eur. J.*, 2007, **13**, 7153.
8 A. H. Lu, E. L. Salabas and F. Schüth, *Angew. Chem., Int. Ed.*, 2007, **46**, 1222.
9 S. G. Kwon and T. Hyeon, *Acc. Chem. Res.*, 2008, **41**, 1696.
10 C. J. Bae, S. Angappane, J. G. Park, Y. Lee, J. Lee, K. An and T. Hyeon, *Appl. Phys. Lett.*, 2007, **91**, 102502.
11 X. H. Li, D. H. Zhang and J. S. Chen, *J. Am. Chem. Soc.*, 2006, **128**, 8382.
12 Z. Li, B. Tan, M. Allix, A. I. Cooper and M. J. Rosseinsky, *Small*, 2008, **4**, 231.
13 L. Zhang, S. Qiao, Y. Jin, H. Yang, S. Budihartono, F. Stahr, Z. Yan, X. Wang, Z. Hao and G. Q. Lu, *Adv. Funct. Mater.*, 2008, **18**, 3203.
14 J. Liu, Z. Sun, Y. Deng, Y. Zou, C. Li, X. Guo, L. Xiong, Y. Gao, F. Li and D. Y. Zhao, *Angew. Chem., Int. Ed.*, 2009, **48**, 5875.
15 S. Laurent, D. Forge, M. Port, A. Roch, C. Robic, L. Vander Elst and R. N. Muller, *Chem. Rev.*, 2008, **108**, 2064.
16 S. H. Sun, H. Zeng, D. B. Robinson, S. Raoux, P. M. Rice, S. X. Wang and G. X. Li, *J. Am. Chem. Soc.*, 2004, **126**, 273.
17 A. H. Latham and M. E. Williams, *Acc. Chem. Res.*, 2008, **41**, 411.
18 J. P. Ge, Y. X. Hu, M. Biasini, W. Beyermann and Y. D. Yin, *Angew. Chem., Int. Ed.*, 2007, **46**, 4342.
19 J. J. Zhu, O. Palchik, S. Chen and A. Gedanken, *J. Phys. Chem. C*, 2000, **104**, 7344.
20 X. H. Liao, J. M. Zhu, J. J. Zhu, J. Z. Xu and H. Y. Chen, *Chem. Commun.*, 2001, 937.
21 D. Zhu, X. Jiang, C. Zhao, X. L. Sun, J. R. Zhang and J. J. Zhu, *Chem. Commun.*, 2010, **46**, 5226.
22 H. Wang, J. M. Zhu, J. J. Zhu, L. M. Yuan and H. Y. Chen, *Langmuir*, 2003, **19**, 10993.
23 H. Wang, J. J. Zhu, J. M. Zhu, X. H. Liao, S. Xu, T. Ding and H. Y. Chen, *Phys. Chem. Chem. Phys.*, 2002, **4**, 3794.
24 B. Zhou and J. J. Zhu, *Nanotech.*, 2009, **20**, 6.
25 R. J. Cui, C. Liu, J. M. Shen, D. Gao, J. J. Zhu and H. Y. Chen, *Adv. Funct. Mater.*, 2008, **18**, 2197.
26 R. M. Xing, X. Y. Wang, L. L. Yan, C. L. Zhang, Z. Yang, X. H. Wang and Z. J. Guo, *Dalton Trans.*, 2009, 1710.
27 M. Descostes, F. Mercier, N. Thromat, C. Beaucaire and M. Gautier-Soyer, *Appl. Surf. Sci.*, 2000, **165**, 288.
28 S. H. Liu, R. M. Xing, F. Lu, R. K. Rana and J. J. Zhu, *J. Phys. Chem. C*, 2009, **113**, 21042.
29 T. K. With, *Biochem. J.*, 1975, **147**, 249.
30 K. Woo, J. Hong, S. Choi, H. W. Lee, J. P. Ahn, C. S. Kim and S. W. Lee, *Chem. Mater.*, 2004, **16**, 2814.
31 C. C. Mi, J. P. Zhang, H. Y. Gao, X. L. Wu, M. Wang, Y. F. Wu, Y. Q. Di, Z. R. Xu, C. B. Mao and S. K. Xu, *Nanoscale*, 2010, **2**, 1141.
32 J. Qin, I. Asempah, S. Laurent, A. Fornara, R. N. Muller and M. Muhammed, *Adv. Mater.*, 2009, **21**, 1354.
33 W. J. Chen, P. J. Tsai and Y. C. Chen, *Small*, 2008, **4**, 485.
34 R. Hirsch, E. Katz and I. Willner, *J. Am. Chem. Soc.*, 2000, **122**, 12053.
35 A. Dyal, K. Loos, M. Noto, S. W. Chang, C. Spagnoli, K. V. P. M. Shafi, A. Ulman, M. Cowman and R. A. Gross, *J. Am. Chem. Soc.*, 2003, **125**, 1684.